



Cite this: *Nanoscale*, 2017, **9**, 1263

A wave-shaped hybrid piezoelectric and triboelectric nanogenerator based on P(VDF-TrFE) nanofibers†

Xuexian Chen,^a Mengdi Han,^b Haotian Chen,^a Xiaoliang Cheng,^b Yu Song,^b Zongming Su,^b Yonggang Jiang^c and Haixia Zhang^{*a,b}

A wave-shaped hybrid nanogenerator (NG) with mutually enhanced piezoelectric and triboelectric output is presented in this work. By sandwiching piezoelectric P(VDF-TrFE) nanofibers between wave-shaped Kapton films, the device forms a three-layer structure, which can generate piezoelectric and triboelectric outputs simultaneously in one press and release cycle. Through systematic situational analysis and experimental validation, the three-layer structure can achieve obvious improvement of the output performance for both parts. When triggered with 4 Hz external force, the piezoelectric part generates a peak output and current of 96 V and 3.8 μ A, which is \sim 2 times higher than its initial output. Meanwhile, the performance of triboelectric parts also increases 8 V and 16 V with the assistance of piezoelectric potential. The enhanced high output enables the hybrid nanogenerator to instantaneously light up LEDs and charges capacitors quickly, which shows extensive application prospects in the field of self-powered systems or sensor networks.

Received 3rd October 2016,
Accepted 18th December 2016

DOI: 10.1039/c6nr07781a

www.rsc.org/nanoscale

Introduction

Among various renewable and sustainable power sources in the ambient environment, mechanical energy is the most widely distributed resource with numerous energy types and scales, such as mechanical vibration, sound, rolling of tires, walking, tides in the ocean. To solve the problem of increasing energy crisis and achieving self-powering low-energy consumption electronics, many kinds of methods have been exploited for effectively converting mechanical energy into electricity, including piezoelectric effect,¹ electrostatic effect,^{2–4} electromagnetism,⁵ *etc.* As each type of generator has its own weakness in practical applications, the concept of harvesting one kind of energy by simultaneously using multi-type generators has been promoted to improve the output of energy harvesters.^{6–9} Since the output characteristic, matched resist-

ance and the working frequency of piezoelectric nanogenerator (PENG) and triboelectric nanogenerator (TENG) are very similar, the combination of both effects is promising to enhance the energy conversion efficiency from the ambient environment. The PENG has the advantages of flexibility and generation of electricity from tiny deformations by employing functional materials such as ZnO,¹⁰ lead zirconate titanate (PZT),¹¹ BaTiO₃,¹² polyvinylidene fluoride (PVDF) and its copolymers and so on.^{13–17} Besides, the TENG initiated by ZL Wang's group in 2012 can also achieve flexibility and high output by combining contact electrification and electrostatic induction,^{18,19} making it a potential choice as a power source for driving electronics or self-powered active sensors for sensing the change of angle,²⁰ humidity,²¹ ion concentration,²² *etc.*

In the previous work, simulation analysis of the coupling between the piezoelectric and triboelectric effects has been promoted showing that the output performance of the piezoelectric–triboelectric hybrid nanogenerator can be enhanced with proper structure design and polarization directions.²³ The coupling can be mainly divided into 3 types:

(1) Add the electrostatic charges directly onto the piezoelectric material surface through contact with other material to enlarge the piezoelectric potential difference between the two surfaces of the piezoelectric film.²⁴

(2) By sharing an electrode between the triboelectric and piezoelectric parts, one can add the triboelectric charges onto the PENG electrode, thus improving the PENG output.^{6,25}

^aAcademy for Advanced Interdisciplinary Studies, Peking University, Beijing 100871, China. E-mail: hxzhang@pku.edu.cn

^bNational Key Lab of Micro/Nano Fabrication Technology, Peking University, Beijing 100871, China

^cSchool of Mechanical Engineering and Automation, Beihang University, Beijing 100191, China

† Electronic supplementary information (ESI) available: Diameter distribution and FTIR spectra of the P(VDF-TrFE) nanofibers, working principle of the PENG and TENG, experimental verification of the simulation results, output performance of the PENG, one single measured waveform of the three generators. See DOI: 10.1039/c6nr07781a

(3) Through rational structure design, the device can generate electric output based on these two effects individually in a single press-and-release cycle, which can improve the efficiency of energy conversion.^{26–28}

However, all of these reported hybrid structures just enhanced the potential at one side of the piezoelectric material. As the polarization of the piezoelectric material is constant, through rational structure design and material selection, the output of piezoelectric and triboelectric parts can be further enhanced when both sides of the piezoelectric material are adopted.

Based on the above ideas, we present a hybrid wave-shaped nanogenerator with mutually reinforced piezoelectric and triboelectric output. A wave-shaped structure is adopted for its built-in space and self-recovery characteristics to increase integration, which is very favorable in assembling TENGs, especially for harvesting water wave energy.^{29,30} A flexible piezoelectric P(VDF-TrFE) nanofiber film fabricated through electrospinning is employed as a major component of the PENG. For the high electric field intensity during the electrospinning process can induce the formation of β -phase crystalline in the P(VDF-TrFE). There is no need to conduct the post polarization process, which simplifies the fabrication procedure a lot.^{31–33} Besides, the P(VDF-TrFE) nanofibers are much more flexible than the commercial PVDF film with the same thickness. Thanks to the flexibility of electrospinning nanofibers, the piezoelectric film can make contact with the electrode conformally. Finite element method (FEM) simulation and experimental tests are conducted to verify the analysis that triboelectric charges and piezoelectric potential can induce charge reversal on the electrodes shared by the PENG and the TENG, which is the main reason for improving output performance of the device. Further systematic tests show that the peak voltages of the PENG, the upper TENG and the lower TENG can reach 96 V, 88 V and 361.27 V, respectively. For applications, the device can light up 75 LEDs and charge capacitors rapidly, verifying the validity of theoretical analysis and structure design.

Experimental details

Fabrication of the piezoelectric P(VDF-TrFE) nanofiber film

The fabrication procedure of the piezoelectric P(VDF-TrFE) nanofibers was based on a far-field electrospinning process. P(VDF-TrFE) composites with a weight ratio of 75/25 were dissolved into the mixture of dimethyl formamide (DMF) and acetone (40 : 60 weight%) at a concentration of 14%, and then was ultrasonically treated at a temperature of 60 °C for 3 h until the solution becomes homogeneous. Subsequently, the solution was filled in a 1.0 ml plastic syringe and fed at a constant speed of 1 ml h⁻¹ through a micro pump. The positive node of a high voltage supply was connected to the syringe needle with application of a bias voltage of around 15 kV. A grounded drum with a diameter of 10 cm covering of a copper film was placed 7.5 cm away from the needle and set at a

rotation speed of 2000 rpm for collection of aligned nanofibers. After continuously collecting for about 2 h, the nanofiber arrays formed a film with a thickness of about 40 μ m. Then the nanofiber film is annealed at a temperature of 85 °C for 2 h to further ensure the P(VDF-TrFE) transformation into its β -phase.

Fabrication of the wave-shaped PENG

An array of glass rods with a diameter of 8 mm was employed to fabricate the wave-shaped structure. The Kapton film mounted onto the rods was placed into an oven and baked at 200 °C for 2 h. Then 200 nm Cu was sputtered on one surface of the Kapton film to form an electrode and a lead wire was connected to it as the output terminal. After that the as-spun P(VDF-TrFE) nanofiber film was transferred and sandwiched between two pieces of such Cu-Kapton films with the conductive copper face to each other for the fabrication of an M-shaped PENG. The two Kapton films with a size of 5 \times 5 cm were fixed tightly and bonded together for forming excellent contact with the piezoelectric film.

Assembling of the hybrid energy harvester

The outside Kapton films of the wave-shaped PENG were employed as the friction layers of the upper and lower TENGs, respectively. A conductive PET-ITO film, which was utilized both as another friction surface and the conductive electrode of the upper TENG, was directly fixed on the upper surface of the wave-shaped PENG. A PDMS film was fabricated on the PET-ITO surface through spin coating and was adhered to the bottom surface of the Kapton film for forming another friction layer of the lower TENG.

Measurement system

The bottom of the hybrid energy harvester was fixed to a certain surface and the top was triggered by a vibration plate to generate periodic deformation of the device. For output characterization, the external force frequency is 4 Hz, while 5 Hz vibration was adopted in the charging capability test. The output current of the device was measured by using a low-noise current preamplifier (Stanford Research SR570) and all the signals were recorded and displayed through a digital oscilloscope (Agilent DSO-X 2014A).

Results and discussion

The structure diagram of the hybrid energy harvester is shown in Fig. 1a consisting of three parts (the PENG, the upper and lower TENGs) that are vertically aligned. The upper TENG is composed of a PET-ITO film and a wave-shaped Cu-Kapton film. The wave-shaped Cu-Kapton film works as one of the friction layer as well as a middle support structure. The conductive ITO film is utilized as both the electrode and the top friction layer as it is easy to lose electrons when it makes contact with Kapton, thus forming a negative electron layer on the surface of the Kapton film. The lower TENG is similar to the

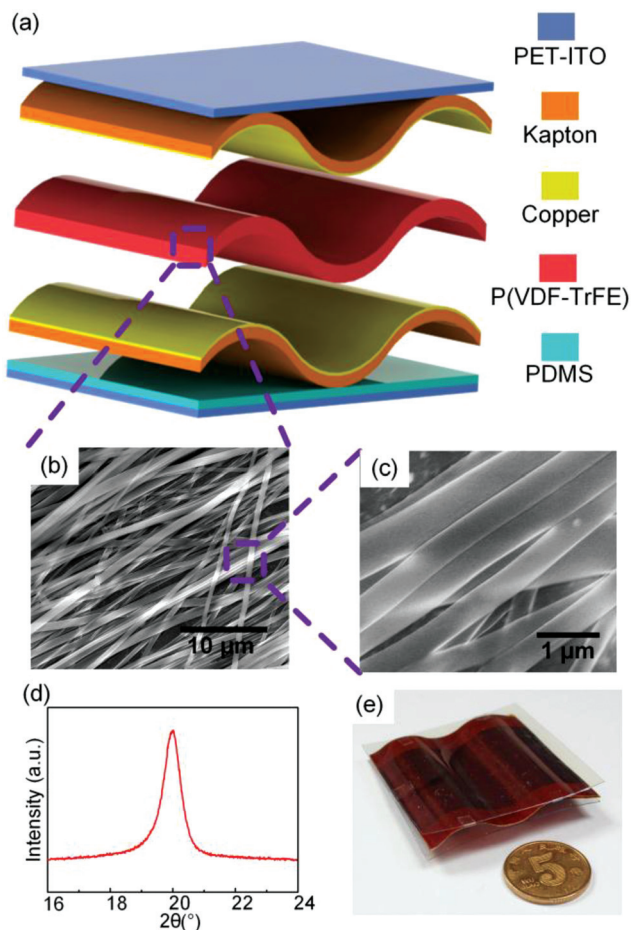


Fig. 1 Structure design of the hybrid NG. (a) Schematic view of the device. (b) SEM image of the fabricated nanofibers. (c) The magnified SEM images of the nanofibers. (d) XRD analysis of the P(VDF-TrFE) nanofibers. (e) Photograph of the fabricated device.

upper one except that a thin PDMS film is coated on the PET-ITO film surface. PDMS is selected as the contact material due to its stronger ability of attracting electrons compared to Kapton in the triboelectric series,¹⁸ thus resulting in the positively charged surface of the Kapton film. The difference of the charge types between the two surfaces of the Kapton film is critical for the enhancement of piezoelectric output performance. The middle part (*i.e.*, the PENG) of the device is composed of the piezoelectric P(VDF-TrFE) nanofiber film as shown in Fig. 1b and c, which is tightly sandwiched between the two Cu-Kapton films. The P(VDF-TrFE) nanofibers are obtained by a far-field electrospinning process with a thickness of 40–80 μm , depending on the collection time duration. The average fibre diameter for materials studied here is 450 nm, with a distribution that appears in Fig. S1(a).[†] Thanks to the excellent flexibility of the P(VDF-TrFE) nanofiber film, the piezoelectric part can be fixed to a wave-shaped structure, meanwhile, retaining the ability of quick shape recovery under deformation, which assures the output performance of the whole device. The X-ray diffraction (XRD) pattern of the

as-spun P(VDF-TrFE) nanofibers is shown in Fig. 1d with a peak identified at 19.9° , corresponding to the dominant β -phase in the P(VDF-TrFE), which is crucial for the piezoelectric output. The Fourier transform infrared (FTIR) spectra shown in Fig. S1(b)[†] also confirms this conclusion. The prepared hybrid energy harvester possesses the advantage of flexibility and a small volume with a uniform size of $5\text{ cm} \times 5\text{ cm} \times 0.5\text{ cm}$, as revealed in Fig. 1e.

Working principle

Fig. 2 demonstrates the working mechanism of the hybrid energy harvester. The mechanism of hybridization is derived from the above mentioned type 2 situation except that the electrostatic charges added to the PENG electrode are induced by the triboelectric charges on the friction layer of the TENG instead of that directly added to the PENG electrode. At the initial state, no charges exist on the surfaces of electrodes (ITO and Cu) and polymers (Kapton and PDMS). After a few cycles of contact and separation, the upper TENG accumulates negative charges on the surface of the Kapton film and the same amount of positive charges on the ITO film while the lower TENG gains positive charges on the surface of the Kapton film and the equal negative charges on the surface of PDMS due to the different electron affinities (Fig. 2a). Because of the connection between two electrodes in each generator, the charges on the electrodes will redistribute in order to screen the electric field of triboelectric charges and reach equilibrium as shown in Fig. 2b. When an external impact is applied on the top surface, the wave-shaped Kapton films is pressed in the vertical direction and the gaps between the two friction layers decrease in the upper and lower TENGs. As a result, the potential difference is diminished between the ITO electrode and Cu on the Kapton film in the upper TENG, driving positive charges to flow from the Cu electrode to the ITO electrode. Similarly, the potential difference between the electrodes in the lower TENG is also decreased but the positive charges flow in the opposite direction (*i.e.*, from the ITO electrode to the Cu electrode on the Kapton film). Meanwhile, the deformation in the wave-shaped structure causes the polarization of the piezoelectric nanofiber film, as shown in Fig. S2,[†] which makes the top surface of the P(VDF-TrFE) film have a higher potential than the bottom one. This piezoelectric potential can affect the charge distribution between the two Cu electrodes, indicating that positive charges tend to transfer from the upper Cu electrode to the bottom Cu electrode. Under the influence of the upper TENG, the lower TENG and the middle PENG, the charges flow forward in external circuits, as shown in Fig. 2c. When the wave-shaped spacer is pressed to the limit, the two friction layers of each TENG make contact with those of the other and the TENGs reach equilibrium. However, the deformation of the piezoelectric film reaches the highest value, thus generating the strongest piezoelectric potential difference between the two surfaces of the P(VDF-TrFE) film. The particular polarization direction of the piezoelectric film leads to the reverse of the charge polarity on the two Cu electrodes, which is shown in Fig. 2d. At this state, the charge distribution

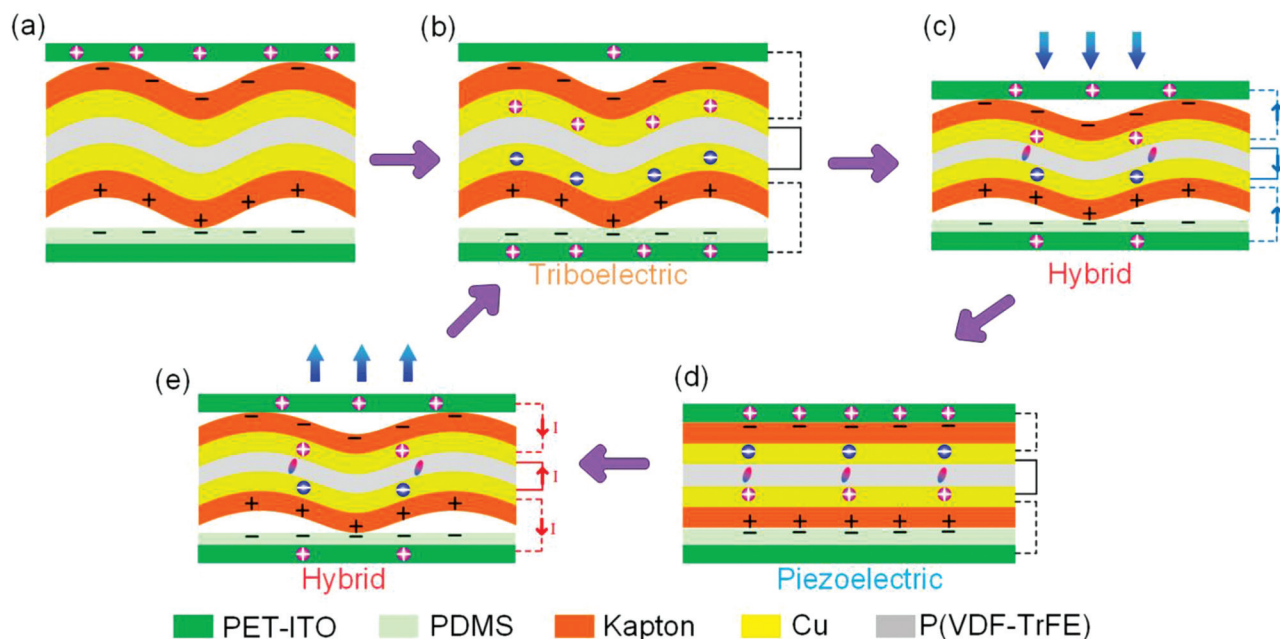


Fig. 2 Working principle of the hybrid NG. (a) Triboelectric charges are generated on the surface of friction layers after several cycles of contact and separation. (b) Released state. The charges reach equilibrium under the electrostatic induction of triboelectric charges. (c) Pressing state. Piezoelectric potential and triboelectric charges simultaneously drive charges to move forward in the external circuits. The charges reach equilibrium induced by piezoelectric potential. (d) Pressed state. (e) Releasing state. Piezoelectric potential gets weakened, driving charges move back through the external circuit.

is mainly induced by the piezoelectric effect. Once the external force is released, the compressed Cu-Kapton film tends to recover to the initial state owing to the elasticity of the designed wavy structure. Consequently, the electric potential difference is generated between the two electrodes of each TENG while the piezoelectric potential decreases, driving the charges to flow back through external circuits (Fig. 2e). During this process, the hybrid NGs react on the electrons together. When the impacted wave-shaped structure reverts to the initial state, the effect of piezoelectric potential disappears and triboelectric charges on the Kapton film will attract or repulse most of the charges to or from the Cu electrode. The charge distribution recovers to the initial state as shown in Fig. 2b and will repeat the cycle from Fig. 2b–e under periodic external impact, thus driving the electrons to go back and forth in the external circuits. The separate enhancement principles of the PENG and TENGs (*i.e.* the triboelectric charges enhance the output of the PENG and the piezoelectric potential enhances the output of TENGs) as well as the interface circuit of the device are shown in Fig. S2.†

Design for the output performance enhancement

Because the working principle and output characteristics of the PENG and TENG show high similarity, the combination of these two types of nanogenerators can bring enhancement of the output through the interaction of the triboelectric and piezoelectric potential. To verify this, FEM simulation is employed to numerically solve the potential and charge distributions of the hybrid system (Fig. 3). The configuration of the

model is the same as the real device except that the wave-shaped piezoelectric film is simplified to a flat film, which better demonstrates the interaction of the piezoelectric and triboelectric effect. The lower surface of top PET-ITO and the lower surface of bottom Kapton are charged with a density of $10 \mu\text{C cm}^{-2}$, respectively, while the upper surface of the top Kapton with a negative charge density of $-10 \mu\text{C cm}^{-2}$. In order to clarify the enhancement effect of the hybrid design, the comparison among three types of charge configuration (only with piezoelectric polarization, only with triboelectric charges and the hybrid mode) is conducted, as shown in Fig. 3a. In the only piezoelectric (PE) polarization mode (Fig. 3a(i)), there is no potential difference in all the electrodes when the device is separated. Similarly, the potential is zero in all the electrodes in the compressed devices when there are only triboelectric (TE) charges (Fig. 3a(ii)). In the hybrid mode (Fig. 3a(iii)), when the gap is zero, the upper Cu electrode has a positive potential while the lower one has a negative potential due to the piezoelectric effect. In contrast, the potential distribution is inverted on these two electrodes because of the electrostatic induction caused by the triboelectric charges, therefore, more electrons can be driven in the external circuit owing to the larger potential difference between the electrodes in every NG.

Fig. 3b reveals the variations of potential difference in each NG (Fig. 3b(i) for the PENG, Fig. 3b(ii) for the upper TENG and Fig. 3b(iii) for the lower TENG) as the changes of the gap distance in these three situations. The red line in every graph represents the potential difference of each NG when there is

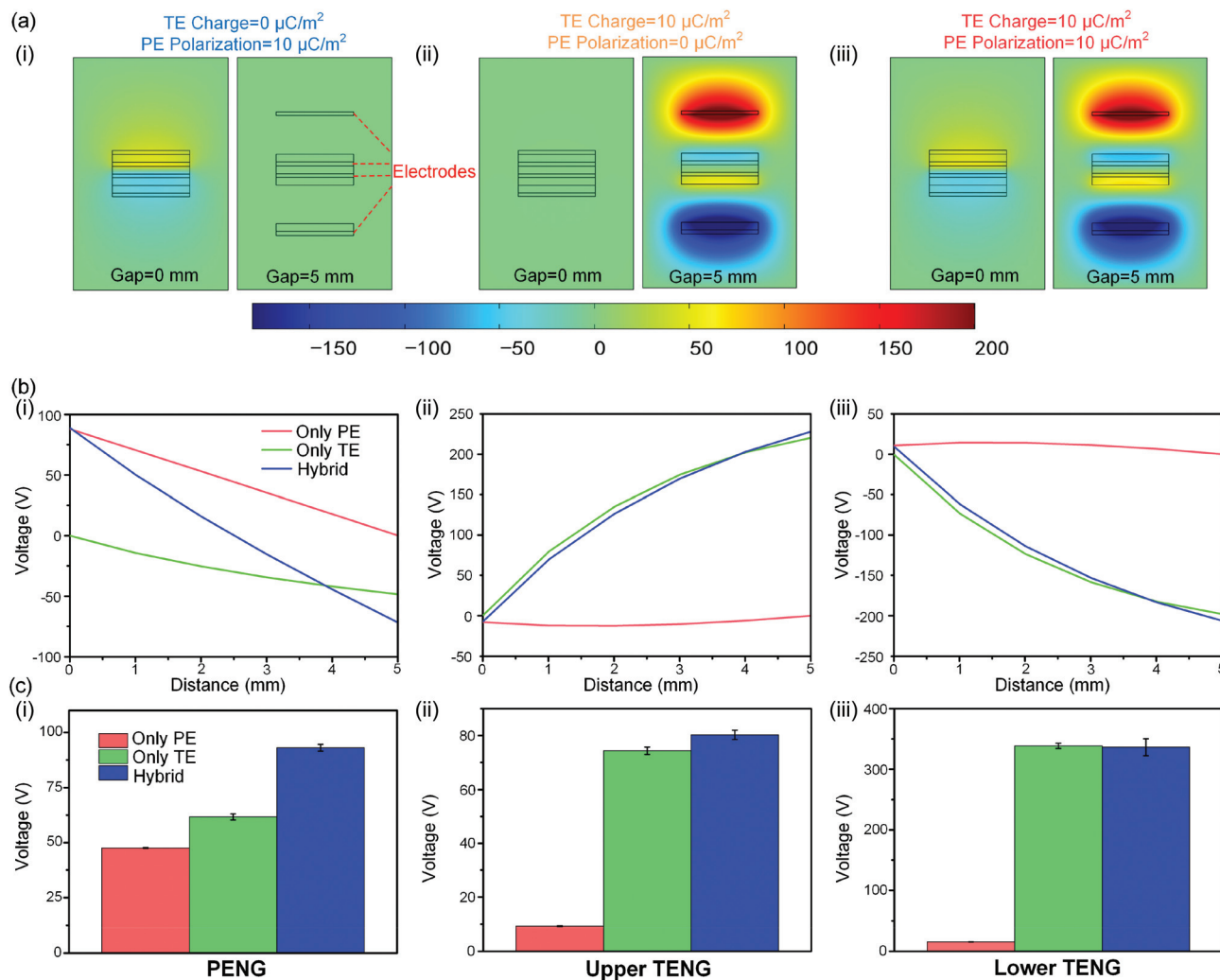


Fig. 3 (a) Simulated potential differences on each electrode under the effects of piezoelectric (i), triboelectric (ii) and hybrid effect (iii). (b) Simulated potential differences between the two electrodes of PENG (i), upper TENG (ii) and lower TENG (iii) under three effects. (c) Measured output voltages of PENG (i), upper TENG (ii) and lower TENG (iii) in three situations.

only PE polarization. The green line is the potential difference when there are only TE charges while the blue line represents the hybrid situation. It is worth noting that, the potential difference changes for every NG in the hybrid mode are larger than the sum of the two individual modes that is caused by the superposition effect of the piezoelectric and triboelectric potential.

Comparative tests are conducted to verify the conclusion of FEM simulation as shown in Fig. S3.† We coated the PET-ITO with the Kapton film in the two TENGs to verify the only PE situation as little triboelectric charge will be generated between the same friction material. P(VDF-TrFE) nanofibers are replaced by paper to verify the only TE situation, therefore no piezoelectric potential will be generated when the device is pressed. The test results are shown in Fig. 3c. As for the PENG part, the peak-peak voltages are 47.8 V, 64 V, and 96 V for the only PE mode, only TE mode and hybrid mode, respectively (Fig. 3c(i)). For the upper TENG, the output voltage is 10.1 V

when there is only piezoelectricity, 86 V when there is only triboelectrification and increased to 88 V when the two parts work together (Fig. 3c(ii)). As shown in Fig. 3c(iii), because of the huge discrepancy between the output of the PENG and the lower TENG, the hybridized output voltage is almost the same with the only TE mode (*i.e.*, 361.27 V).

In summary, the enhanced output of each NG consists of two parts. The first part is the original piezoelectric or triboelectric output. The second part is the induced charges on the electrode caused by the triboelectric charges or the piezoelectric potential, which contribute to the enhancement.

Output characterization

Before the measurement of the device, the output performance of the wave-shaped P(VDF-TrFE) nanofiber film is evaluated to verify its piezoelectric performance and verify the polarization direction, which is shown in Fig. S4 and S5.† To quantitatively evaluate the output performance, the electric output of the

hybrid NG was systematically measured under periodic external force, as shown in Fig. 4. The bottom of the device is fixed to a certain surface while the top surface is triggered by a sinusoidal vibrating plane. For the output voltage and current measurement, the vibration frequency is set to 4 Hz and the displacement amplitude of the top surface is 0.4 cm, which just corresponds to the thickness of the device. Given that the device is composed of three energy harvesting parts, we characterize their electric output individually. As shown in Fig. 4a–c, the peak voltages of the PENG, the upper TENG and the lower TENG of the device reach up to 96 V, 88 V and 361.27 V with a load resistance of 100 M Ω , respectively. This high PENG output is owing to the hybridization of the PENG and TENGs, which has been discussed before. The output voltage of the TENG can be derived from the equation:³⁴

$$V = -\frac{Q}{S\epsilon_0}(d_0 + d) + \frac{\sigma d}{\epsilon_0} \quad (1)$$

where ϵ_0 is the permittivity of air, σ , d , d_0 , are the charge density, gap distance changes and effective gap distance of friction layers, S and Q are the area and transfer charge of the

TENG. The large output disparity between the two TENG parts (the value for the bottom one is about 4 times that of the upper one) is mainly due to the friction property differences of ITO and PDMS materials as well as the structure design. When the device is in the released state, the M-shaped Kapton film at a larger distance with the PDMS film compared with the ITO film. For the output current, all parts are measured using a 1 Ω external resistance. As shown in Fig. 4d–f, the peak current of the PENG, the upper TENG and the lower TENG are 3.8 μA , 3.68 μA and 10.85 μA , respectively. The current difference between the PENG and the lower TENG is not as large as the voltage, owing to the fact that the PENG has a relatively lower equivalent resistance than that of the lower TENG.³ The specific relationship between the measured signals of the device in one single cycle and the working mechanism is shown in Fig. S6.†

To investigate the dependence of the output power of the three NGs on load resistance, the output current and power values under 5 Hz external force are measured with different resistances (ranging from 100 k Ω to 1 G Ω) connected in the circuit (Fig. 4g–i). For all the parts, the output current

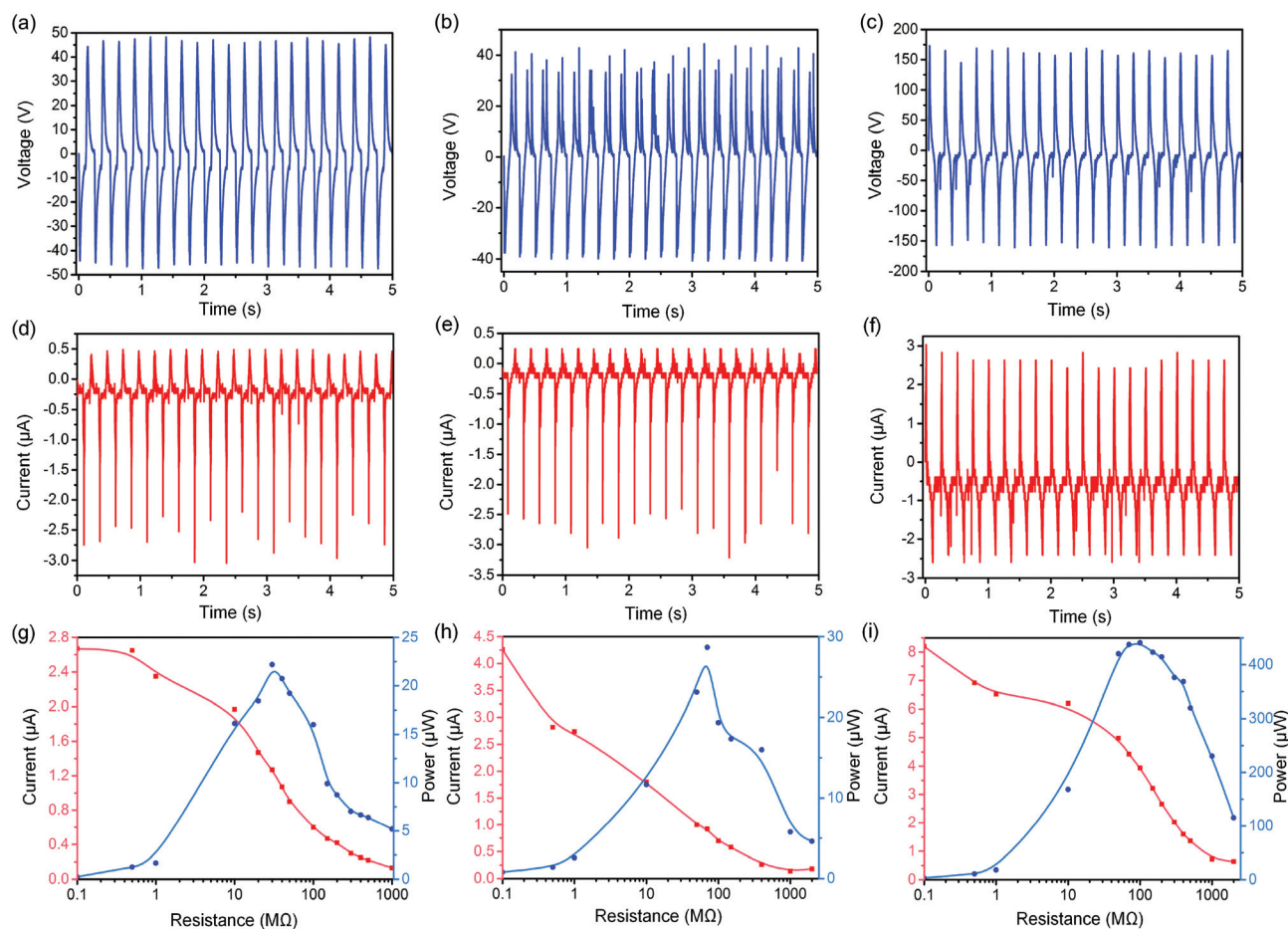


Fig. 4 Output characterization. The output voltage of the PENG (a), upper TENG (b) and lower TENG (c). The output current of the PENG (d), upper TENG (e), and lower TENG (f). Instantaneous power changes with the increasing load resistance for the PENG (g), upper TENG (h), and lower TENG (i).

continuously decreased with the increase of the resistance. In comparison, the instantaneous output power reaches a maximum value at a certain resistance, that is, 22.18 μW at 30 M Ω for the PENG part, 28.67 μW at 70 M Ω for the upper TENG and 441 μW at 100 M Ω for the lower TENG, respectively.

Applications

To demonstrate the practical applications in powering micro-electronic devices, the output voltage of the hybrid energy harvester is first rectified to instantaneously light up commercial light-emitting diodes (LEDs) (Fig. 5a). The hybrid energy harvester is a four terminal device with two Cu electrodes shared by the PENG and TENGs. To avoid charges cancelling each other between different nanogenerators, rectifiers are used for each part to achieve electrical isolation. Fig. 5b–d show the rectified voltages and lighted LEDs of the PENG part, the TENG parts (the parallel connection of the upper TENG and the lower TENG) and the whole device, respectively. Under the periodical external force, partial of the LEDs are lighted up

by the PENG due to the limited output. Although all the 75 LEDs can be lighted by the TENG part, the brightness is not as high as in the case where all three parts are connected. In more practical situations, the microelectronic devices require a constant DC source to be powered up. In that case, the pulse output of the generators need to be stored in a capacitor or Li-battery. Therefore, charging ability of the hybrid NGs is tested as shown in Fig. 5e. In the experiment, a 5 Hz external force is applied to the device. Then the generated voltage is rectified to continuously charge a 1 μF capacitor. During the charging time of 1 min, voltages of 3.9 V, 19.2 V and 25 V are achieved for the piezoelectric part, the triboelectric part and the whole device, respectively. These demonstrations prove the capability of the hybrid energy harvester as a sustainable power source.

Conclusion

In summary, we design a flexible hybrid energy harvester based on piezoelectric and triboelectric effects as a sustainable power source. By employing flexible P(VDF-TrFE) nanofibers and the thermally shaped Kapton film to form a wave-shaped supporting structure, we combine the piezoelectric NG and triboelectric NG together and achieve the effect of interaction enhancement. Under a 4 Hz periodic external force, the piezoelectric NG can generate a peak voltage and current of 96 V and 3.8 μA , respectively. For the upper TENG, the output voltage is 88 V and the current is 3.68 μA , while the values are 361.27 V and 10.85 μA , respectively. Through FEM simulation and experiment verification, the output of the PENG is enhanced by almost 2 times (from 47.8 V to 96 V) by combining with triboelectric charges. Similarly, the output of the triboelectric part also benefits from the piezoelectric potential, increasing from 80.27 V to 88.33 V for the upper TENG and from 345.4 V to 361.27 V for the lower TENG. This is a simple and cost-effective method that realizes the output enhancement of both the piezoelectric and triboelectric NGs. The high output enables the hybrid energy harvester to be used as a power source for lighting LEDs or charging capacitors, which shows great potential in the field of self-powered systems or sensor networks.

Acknowledgements

This work is supported by the National Natural Science Foundation of China (Grant No. 61674004 and 91323304), the National Key R&D Project from Minister of Science and Technology, China (2016YFA0202701), and the Beijing Science & Technology Project (Grant No. D151100003315003) and the Beijing Natural Science Foundation of China (Grant No. 4141002).

The authors also want to thank Y. G. Jiang and L. L. Gong of Beihang University for help, the fabrication of P(VDF-TrFE) nanofibers was carried out at the Bionic and Micro/Nano/

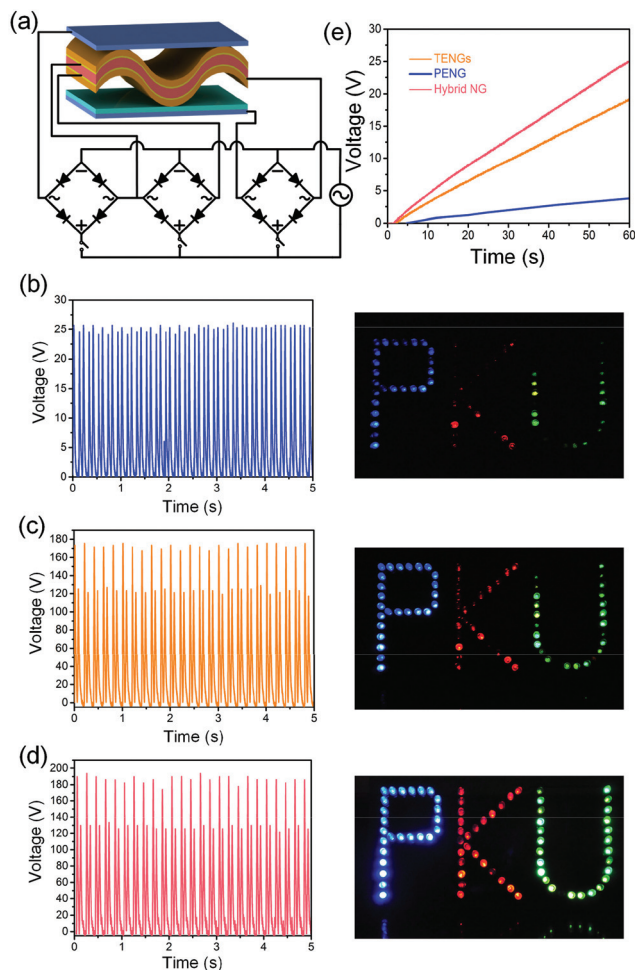


Fig. 5 (a) The circuit diagram of the hybrid NG for lighting up LEDs. (b)–(d) Rectified output voltage and the lighted up LEDs of PENG, upper TENG and lower TENG, respectively. (e) Charging ability test of the hybrid NG.

Bio Manufacturing Technology Research Center in Beihang University.

Notes and references

- 1 R. Elfrink, T. M. Kamel, M. Goedbloed, S. Matova, D. Hohlfeld, Y. van Andel and R. van Schaijk, *J. Micromech. Microeng.*, 2009, **19**, 094005.
- 2 F. R. Fan, Z. Q. Tian and Z. Lin Wang, *Nano Energy*, 2012, **1**, 328.
- 3 X. S. Zhang, M. D. Han, R. X. Wang, F. Y. Zhu, Z. H. Li, W. Wang and H. X. Zhang, *Nano Lett.*, 2013, **13**, 1168.
- 4 P. Basset, D. Galayko, M. Paracha, F. Marty, A. Dudka and T. Bourouina, *J. Micromech. Microeng.*, 2009, **19**, 115025.
- 5 S. P. Beeby, R. N. Torah, M. J. Tudor, P. Glynne-Jones, T. O'Donnell, C. R. Saha and S. Roy, *J. Micromech. Microeng.*, 2007, **17**, 1257.
- 6 M. Han, X. S. Zhang, B. Meng, W. Liu, W. Tang, X. Sun, W. Wang and H. Zhang, *ACS Nano*, 2013, **7**, 8554.
- 7 B. Zhang, J. Chen, L. Jin, W. Deng, L. Zhang, H. Zhang, M. Zhu, W. Yang and Z. L. Wang, *ACS Nano*, 2016, **10**, 6241.
- 8 C. Zhang, Z. H. Zhang, X. Yang, T. Zhou, C. B. Han and Z. L. Wang, *Adv. Funct. Mater.*, 2016, **26**, 2554.
- 9 Y. Zi, L. Lin, J. Wang, S. Wang, J. Chen, X. Fan, P. K. Yang, F. Yi and Z. L. Wang, *Adv. Mater.*, 2015, **27**, 2340.
- 10 Z. L. Wang and J. Song, *Science*, 2006, **312**, 242.
- 11 X. Chen, S. Xu, N. Yao and Y. Shi, *Nano Lett.*, 2010, **10**, 2133.
- 12 K. Park, S. Xu, Y. Liu, G. Hwang, S. L. Kang, Z. L. Wang and K. J. Lee, *Nano Lett.*, 2010, **10**, 4939.
- 13 C. Chang, V. H. Tran, J. Wang, Y. K. Fuh and L. Lin, *Nano Lett.*, 2010, **10**, 726.
- 14 S. H. Bae, O. Kahya, B. K. Sharma, J. Kwon, H. J. Cho, B. Ozyilmaz and J. H. Ahn, *ACS Nano*, 2013, **7**, 3130.
- 15 J.-H. Lee, K. Y. Lee, B. Kumar, N. T. Tien, N.-E. Lee and S.-W. Kim, *Energy Environ. Sci.*, 2013, **6**, 169.
- 16 X. Chen, H. Tian, X. Li, J. Shao, Y. Ding, N. An and Y. Zhou, *Nanoscale*, 2015, **7**, 11536.
- 17 L. Persano, C. Dagdeviren, Y. Su, Y. Zhang, S. Girardo, D. Pisignano, Y. Huang and J. a. Rogers, *Nat. Commun.*, 2013, **4**, 1633.
- 18 Z. L. Wang, *ACS Nano*, 2013, **7**, 9533.
- 19 X. L. Cheng, L. M. Miao, Z. M. Su, H. T. Chen, Y. Song, X. X. Chen and H. X. Zhang, *Microsyst. Nanoeng.*, 2016, **2**, DOI: 10.1038/micronano.2016.74.
- 20 M. D. Han, X. S. Zhang, X. Sun, B. Meng, W. Liu and H. Zhang, *Sci. Rep.*, 2014, **4**, 4811.
- 21 V. Nguyen and R. Yang, *Nano Energy*, 2013, **2**, 604.
- 22 Z. Lin, G. Zhu, Y. S. Zhou, Y. Yang, P. Bai, J. Chen and Z. L. Wang, *Angew. Chem., Int. Ed.*, 2013, **52**, 5065.
- 23 M. Han, X. Chen, B. Yu and H. Zhang, *Adv. Electron. Mater.*, 2015, **1**, 1500187.
- 24 H. Kim, S. M. Kim, H. Son, H. Kim, B. Park, J. Ku, J. I. Sohn, K. Im, J. E. Jang, J.-J. Park, O. Kim, S. Cha and Y. J. Park, *Energy Environ. Sci.*, 2012, **5**, 8932.
- 25 W. S. Jung, M. G. Kang, H. G. Moon, S. H. Baek, S. J. Yoon, Z. L. Wang, S. W. Kim and C. Y. Kang, *Sci. Rep.*, 2015, **5**, 9309.
- 26 X. Li, Z. H. Lin, G. Cheng, X. Wen, Y. Liu, S. Niu and Z. L. Wang, *ACS Nano*, 2014, **8**, 10674.
- 27 Y. Yang, H. Zhang, S. Lee, D. Kim, W. Hwang and Z. L. Wang, *Nano Lett.*, 2013, **13**, 803.
- 28 X. Wang, B. Yang, J. Liu, Q. He, H. Guo, C. Yang and X. Chen, 2015 28th IEEE International Conference on Micro Electro Mechanical Systems (MEMS), IEEE, 2015, pp. 110–113.
- 29 Y. Su, X. Wen, G. Zhu, J. Yang, J. Chen, P. Bai, Z. Wu, Y. Jiang and Z. Lin Wang, *Nano Energy*, 2014, **9**, 186.
- 30 L. M. Zhang, C. B. Han, T. Jiang, T. Zhou, X. H. Li, C. Zhang and Z. L. Wang, *Nano Energy*, 2016, **22**, 87.
- 31 V. Sencadas, C. Ribeiro, I. K. Bdikin, A. L. Kholkin and S. Lanceros-Mendez, *Phys. Status Solidi A*, 2012, **209**, 2605.
- 32 J. S. Andrew and D. R. Clarke, *Langmuir*, 2008, **24**, 8435.
- 33 A. Baji, Y. W. Mai, Q. Li and Y. Liu, *Nanoscale*, 2011, **3**, 3068.
- 34 S. Niu, S. Wang, L. Lin, Y. Liu, Y. S. Zhou, Y. Hu and Z. L. Wang, *Energy Environ. Sci.*, 2013, **6**, 3576.